Global NEST Journal, Vol 26, No X, pp 1-8

Chitosan-doped ZnO nanoparticles for antibacterial, antifungal, and food preservation applications

Muhammad Junaid Khan[1], Saba Saeed[1]*, Muhammad Javed[2], Waheed Qamar khan[3], M. Anis-ur-Rehman[4], Reem A. Aljeidi[5], Saeedah Musaed Almutairi[5], Monika Toleikiene[6], Rabia Ejaz[7] and Rashid Iqbal[8]*

[1]Institute of Physics, The Islamia University of Bahawalpur-63100, Pakistan
[2]Muhammad Nawaz Sharif University of Engineering and Technology, Multan-60800, Pakistan
[3]Institute of Advanced Materials, Bahauddin Zakariya University, Multan-60800, Pakistan
[4]Applied Thermal Physics Laboratory, Department of Physics, COMSATS University Islamabad-45550, Pakistan
[5]Department of Botany and Microbiology, College of Science, King Saud University, P.O. 2455, Riyadh 11451, Saudi Arabia
[6]Institute of Agriculture, Lithuanian Research Centre for Agriculture and Forestry, Instituto Al. 1, LT-58344 Akademija, Kedainiai, Lithuania
[7]Frontiers Science Center for Rare Isotopes & School of Nuclear Science and Technology, Lanzhou University, Lanzhou 730000, China
[8]Department of Agronomy, Faculty of Agriculture and Environment, The Islamia University of Bahawalpur-63100, Pakistan
Received: 18/02/2024, Accepted: 02/03/2024, Available online: 07/04/2024
*to whom all correspondence should be addressed: e-mail: saba.saeed@iub.edu.pk; rashid.iqbal@iub.edu.pk
https://doi.org/10.30955/gnj.005831

Graphical abstract

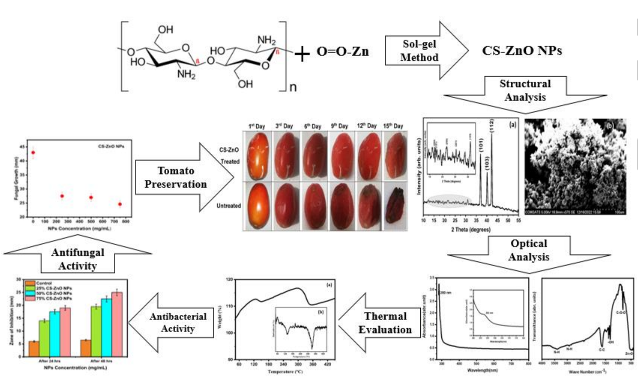

Abstract

Chitosan-doped zinc oxide nanoparticles (CS-ZnO NPs) were meticulously fabricated using the sol-gel methodology. The CS-ZnO NPs underwent comprehensive analytical assessments, employing advanced techniques, encompassing X-ray diffraction (XRD), scanning electron microscopy (SEM), UV visible (UV-Vis) spectroscopy, Fourier-transform infrared (FTIR) spectroscopy, and thermogravimetric analysis (TGA). An average crystallite size of 15 nm was calculated through XRD. These NPs showed an absorption band at 292 nm. TGA revealed the two-phase weight loss mechanism in the investigated nanocomposite. Effective antibacterial activity, at various NPs concentrations, was observed against *Xanthomonas axanopodis pv punicea* and inhibition zones of 19.5 mm, 22.5 mm, and 26 mm were calculated for 25%, 50%, and 75% NPs concentrations respectively after 48 hours of the trial. For the antifungal impact of the CS-ZnO NPs against *Alternaria solani*, rigorous scrutinization was performed via the agar well diffusion method. Within the vicinity of varying dosages, effective zones of 43 mm, 27.5 mm, 27 mm, and 24.6 mm indicated diverse degrees of antifungal activity. Finally, same NPs were employed as food protection agents and tomatoes were used for the purpose. Tomatoes coated with NPs showed better preservation and longer shelf life.

Keywords: Chitosan; nanoparticles; antibacterial; antifungal; food preservation

1. Introduction

Meticulously executed manipulative methodologies, which lead to nanomaterials possessing optimal size and attributes, are an imperative necessity. At the same time, it is imperative to employ environmentally sustainable chemicals. The domain of particulate materials, entailing the science and technology thereof, is progressing astonishingly. NPs, in particular, are garnering ever-increasing global attention (Wang *et al*. 2022; Wasilewska *et al*. 2023). Chitin, a naturally abundant substance, transforms chitosan, a specific type of linear cationic polysaccharide. CS, naturally occurring and possessing an alkaline nature, is sourced from the exoskeletons of marine crustaceans such as prawns and crabs. It has been empirically substantiated to manifest diverse biological functionalities (Dong *et al*. 2022; Gao and Wu 2022).

CS, an adaptable biopolymer, undergoes modification to yield CS-NPs and are recognized for their exceptional attributes as are prominent nanomaterial additives that impart diverse properties of biocomposites. Various methodologies, including emulsification, microemulsion/reverse micelle techniques, precipitation/coacervation processes, and tripolyphosphate cross-linking, facilitate the extraction of CS-NPs. Notably, chitin, found in specific fungal membranes and seafood shells, necessitates chemical transformation to produce CS polymers. These CS-NPs are valued for their functionality, biodegradability, compatibility, safety, and potential antibacterial qualities, rendering them promising bio-based nanomaterials tailored for various applications (Garavand *et al*. 2022; Garavand *et al*. 2017; Mirzaei-Mohkam *et al*. 2019).

Lately, metal-based nanomaterials have garnered considerable attention due to their remarkably precise physicochemical characteristics and their myriad potential applications spanning technology, agriculture, healthcare, food safety, environmental remediation, and many more (Ahmad & Sarbon 2021; Medina *et al*. 2019; Verma *et al*. 2022). With a projected global annual production ranging from approximately 550 to 33,400 metric tons, ZnO NPs stand as the third most extensively employed metal-based NPs within the realm of nanomaterials (Bondarenko *et al*. 2013). Zinc exposure lowers growth in main carp species, reducing feed conversion ratio and organ health, implying ambient zinc levels (Malik *et al*. 2022). In recent times, ZnO NPs have attracted increased interest as a potential substitute in various sectors like optical science, electronics, food packaging, and pharmaceuticals, owing to their biocompatibility, low toxicity, and cost-effectiveness. Many studies have revealed that Zn ions play a pivotal role in inducing cellular demise by stimulating the generation of toxic Zn^{2+} ions and reactive oxygen species. However, it is important to note that the clinical utility of ZnO NPs is restricted by the toxicity associated with their manufacturing processes (Alhujaily *et al*. 2022; Singh *et al*. 2018).

Bacteria make you sick, disrupt your body, and even kill you. Antibacterial therapy can help mitigate these effects (Shaukat *et al*. 2023). The heightened antibacterial effectiveness of nano-sized antibacterial agents primarily arises from their increased surface-to-volume ratio and enhanced surface reactivity. Investigations have unveiled those NPs, including ZnO and CS, which exhibit remarkable antibacterial properties against both Gram-positive and Gram-negative bacteria (Ahmad & Sarbon 2021; Medina *et al*. 2019). Bacteria create distinct compounds that help in their characterization and identification in microbiology (Muhammad *et al*. 2022). CS exhibits inherent natural antibacterial properties, effectively curbing the proliferation of a diverse spectrum of bacteria. This renders it a lucrative option for applications across a wide array of sectors, including but not limited to medication management, wound treatment, and reconstructive surgery (Gasti *et al*. 2022).

The antifungal properties of ZnO have found practical application in traditional craftsmanship, yielding favorable results in terms of enhancing the economic value of indigenous products. This is achieved through the incorporation of ZnO in sunscreens and fungal protection medicines. The mechanism underlying the fungus inhibition by CS-modified ZnO is associated with the response of fungal hyphae to stress and the generation of hydrogen peroxide (Pholnak *et al*. 2020). These nanocomposites showed antifungal properties against Candida albicans and hence proved to be a good candidate for such activities (Dananjaya *et al*. 2018). The growing world population requires more food. To fulfill demand, grow more wheat and other food crops (Farrukh Saleem *et al*. 2022). Fruits are nutrient-dense, including minerals, vitamins, and fiber that are necessary for good health (Bilal Shahid *et al*. 2021).

Efforts to extend the shelf life of vegetables, fruits, and various food items, ensuring both safety and nutritional quality over an extended period, have garnered global interest among experts. For years, nanotechnology has played an important role in this research domain. It is reported that the nanostructures based on ZnO nanorods along with CS could prolong the shelf life of tomatoes (Iqbal *et al*. 2022; Li *et al*. 2021).

A compelling facet of the current study lies in the influence of CS- ZnO NPs on *X. axonopodis pv. Punicae* baterial strain. Notably, this bacterium is responsible for causing pomegranate bacterial blight, a significant affliction in the realm of pomegranate cultivation. The study also delves into the ramifications of the growth of *Alternaria solani*, which is the causative agent behind maladies affecting tomatoes, eggplants, and various other vegetable crops. Additionally, the investigation encompasses an exploration of the impact of CS-ZnO NPs coatings on tomato preservation during subsequent storage. Moreover, this work emphasizes the analysis of the optical, thermal, and morphological properties of CS-ZnO NPs.

2. Materials and methods

2.1. Materials

CS powder, acetic acid (CH_3COOH, 99.5%), hydrogen peroxide (H_2O_2, 98%), sodium hydroxide (NaOH, 97%), zinc acetate dihydrate ($Zn(CH_3COO)_2{\cdot}2H_2O$, 99%), methylene blue ($C_{16}H_{18}ClN_3S$, 82%), and dimethyl sulfoxide (DMSO, 99%) were purchased from Sigma-Aldrich.

2.2. Preparation of CS-ZnO NPS by Sol-Gel

A 1.0 % (w/v) solution of CS was made by dissolving it in a 1% (v/v) acetic acid. After sufficient dissolving, 45 mL of 0.1 M $Zn(CH_3COO)_2{\cdot}2H_2O$ was added to 5 mL of chitosan solution. The combinations' pH was adjusted by adding 0.1 M NaOH and constantly mixing for 4 hours at 85°C to get a pH of 9–10. Later, drying was done at 120°C for 2.5 hours and then annealed for 4 hours at 450°C to achieve $CS_{0.1}ZnO_{0.9}$(CS-ZnO) NPs.

2.3. Characterization and Instrumentation

XRD was employed to discern the crystal structure of the CS-ZnO NPs. Diffraction patterns were acquired within the 2θ range spanning from 10° to 55°. The XRD analysis was conducted using Cu-K radiation (BTX-646) at 50 kV and 40 mA. Shimadzu-1800 UV-Vis spectrometer was used to record the absorbance of the synthesized CS-ZnO NPs within the wavelength range of 280-800 nm. FTIR spectroscopy was executed with the Shimadzu FTIR-8400 model over a range of 400–4000 cm^{-1}. SEM (SU-1500) was employed to examine the structure of nanoparticles, The assessment of the thermal stability of CS-ZnO NPs was carried out using a TGA (STA 449 F3 version). This involved a temperature program spanning from 60-540°C, with a heating rate of 10°C/min, and a flow rate of 50 mL/min in an air environment. The antibacterial evaluations targeted X. axanopodis pv punicea, a Gram-negative bacterium. The Agar Plate Method (MIR-154-PE) was utilized to assess the antibacterial performance of the sample. In addition, the antifungal effects of *Alternaria solani* were investigated via the agar well diffusion technique.

To access food prevention, tomatoes underwent a sequence of procedures. Initially, they were cleaned and disinfected utilizing colloidal silver solution, followed by draining to eliminate the excess water. Subsequently, treatment was administered by immersing the tomatoes in water, draining them, and allowing them to dry in air at room temperature. To gauge alterations in the tomato surface color, an Agrocolor colorimeter was employed. This involved calibrating a white Teflon plate and recording the red component (R) and green component (G), which were then interpreted according to the CIE Lab scale [L* (lightness), a*(red-green color component)]. The texture characteristics of the tomatoes, encompassing hardness and compression load, were evaluated through puncture and compression tests utilizing a Brookfield CT3 texture meter. The pH of the tomatoes was measured using an HI 208 P.H meter. Additionally, a calibration curve for lycopene was established by utilizing a Genesys 10S UV-Vis spectrophotometer at a wavelength of 503 nm.

3. Results and discussion

3.1. Structural analysis

XRD analysis determines the structure of the synthesized material and confirms the nanocomposite's successful fabrication. The XRD pattern is depicted in Figure 1(a), where clear crystal peaks are observed on top of amorphous features. The prepared sample indicated the amorphous and crystalline nature of CS. Inset of Figure 1(a) indicates the XRD peaks at 16.8°, 17.4°, 21.6°, 25.4°, and 30.9° corresponding to (002), (121), (200), (221), and (123) planes, respectively. These planes are typical for CS, which has an orthorhombic structure with lattice parameters a = 8.2, b = 16.4, and c = 10.3, under the JCPD card: 00-039-1894. Three XRD peaks at 36.9°, 40°, and 42.5° are for ZnO assigned to the (101), (103), and (112) planes, respectively, and had a hexagonal wurtzite structure, corresponding to previous studies (Zaman *et al*. 2022). The presence of both phases in the XRD pattern indicates the successful fabrication of CS-ZnO NPs. The crystallite size of the NPs was calculated using the Scherrer formula (Tamanna *et al*. 2024).

$$D = k\lambda / \beta \cos\theta$$

where D is the crystallite size, k is a constant, λ is the wavelength of X-ray Cu (kα) radiation (0.154056 nm), β is the full width at half-maximum, and θ is the Bragg's angle.

The average crystallite size of CS-ZnO NPs was calculated to be ~15 nm. Figure 1(b) displays an SEM image of CS-ZnO NPs. Clear agglomeration with irregular particle shapes, sometimes appearing spherical and oval, with numerous pores are observed. These findings align with prior studies (Islam *et al*. 2024; Rumi & Rahman 2023; Thirumavalavan *et al*. 2013). With the given magnification, the average grain size of the NPs as calculated through ImageJ software was 400 nm.

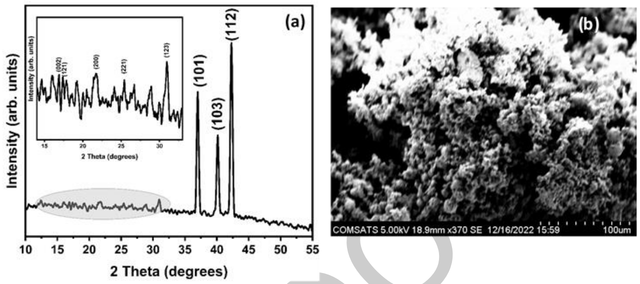

Figure 1. XRD pattern (a) and SEM image (b) of CS-ZnO NPs

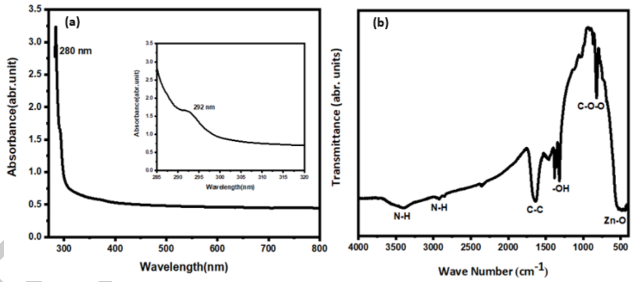

Figure 2. UV-vis absorption curve (a) and FTIR pattern (b) of CS-ZnO NPs

3.2. Optical analysis

Figure 2(a) displays the UV-Vis absorption spectrum of CS-ZnO NPs the sample showed continuous absorption within the whole range of measuring wavelength. This continuous absorption could be assigned to the presence of amorphous CS in the sample. At the same time, two clear absorption bands could be seen in the graph. The initial intense absorption band around 280 nm is associated with the absorption of glass material on which the CS-ZnO sample was mounted. The other absorption band around 292 nm is associated with the CS-ZnO NPs (Arab-Bafrani *et al*. 2021; Khazaal *et al*. 2020; Rilda *et al*. 2022). The FTIR analysis, in Figure 2(b), revealed the material's composition, revealing it to be a CS-ZnO nanocomposite. The spectrum showed distinct peaks, each of which represented a different functional group within the composite. The strong signal at 3394 cm^{-1} indicated N-H stretching, which was associated with the amino groups (NH_2) of CS, confirming its presence. The peak at 2950 cm^{-1} demonstrated C-H stretching vibrations, most likely from aliphatic hydrocarbon groups in CS. The 1650 cm^{-1} peak indicated the presence of carbon-carbon double bonds (C=C), showing the existence of unsaturated groups in CS. The signal at 1375 cm^{-1} showed -OH bending vibrations, indicating hydroxyl groups (OH) found in CS and metal oxides such as ZnO. The 820 cm^{-1} peak indicated the presence of a carbonate group (C-O-O), which could have resulted from CO_2 interactions during synthesis. Finally, the 525 cm^{-1} peak confirmed Zn-O stretching vibrations, which are common in ZnO (Alshammari 2022; Magesh *et al*. 2018; Muiz *et al*. 2022; Nandiyanto *et al*. 2019).

3.3. Thermal analysis

Thermal stability studies on CS-ZnO NPs utilized TGA-DTA analysis, where TGA monitors weight changes with temperature, indicating decomposition or phase transitions, and DTA detects temperature differences, revealing exothermic or endothermic reactions. Weight losses at 150°C and 350°C are shown in Figure 3 (a, b) as 0.88% and 6.2%, respectively. CS exhibits a two-step weight loss: first, water evaporation up to 150°C, followed by CS degradation between 170°C and 350°C. The interaction between water molecules and CS's hydroxyl and amino groups forms hydrogen bonds, affecting thermal behavior. While chitosan degradation (170-350°C) is exothermic and dependent on ZnO concentration and hydrogen bonds with water molecules, water evaporation (~150°C) is endothermic (Corazzari *et al*. 2015; Domyati 2024; González-Campos *et al*. 2010; Prokhorov *et al*. 2020; Yempally *et al*. 2024).

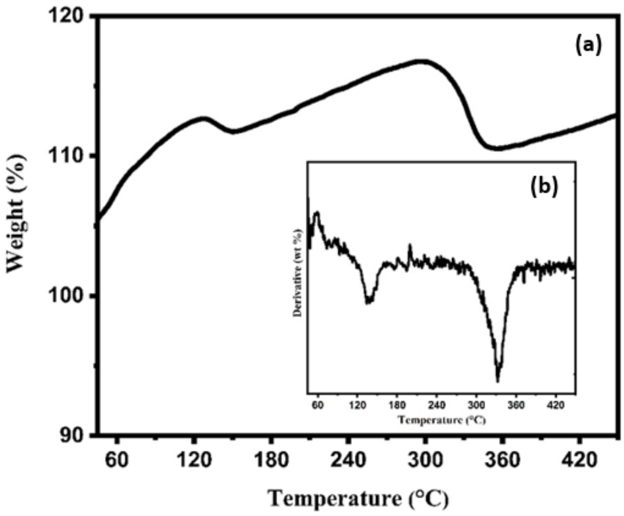

Figure 3. TGA curve (a) and DTA curve (b) of CS-ZnO NPs

3.4. Antibacterial activity

Figure 4 depicts the inhibition zone diameter versus three different concentrations of CS-ZnO NPs. The inhibition zone was calculated after 24 and 48 hours of trial and it was observed that increasing the NPs concentration increases the inhibition effect against Gram-negative bacteria (*X. axanopodis pv punicea*). The primary mechanisms behind antibacterial activity include cell wall disruption and membrane damage (Nandana *et al*. 2021). Metal-Zn adhesion to the cell membrane initiates the interaction between nano-Zn and bacteria, causing morphological changes, membrane depolarization, and subsequent intracellular leakage, ultimately leading to cell death (Fayaz *et al*. 2010). The increased bactericidal efficacy of the CS-ZnO NPs is due to amino groups interacting with the negatively charged carboxylic acid in the bacterial cell wall and hence increasing the microbial death (Madhan *et al*. 2021; Ramezani *et al*. 2019; Yue *et al*. 2021).

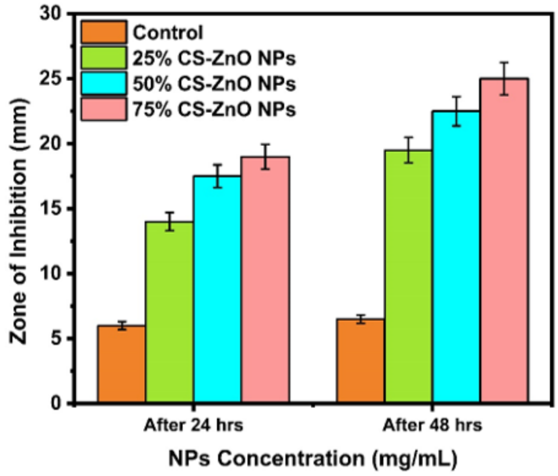

Figure 4. Antibacterial activity CS-ZnO NPs at three different NPs concentrations against X. axanopodis pv punicea

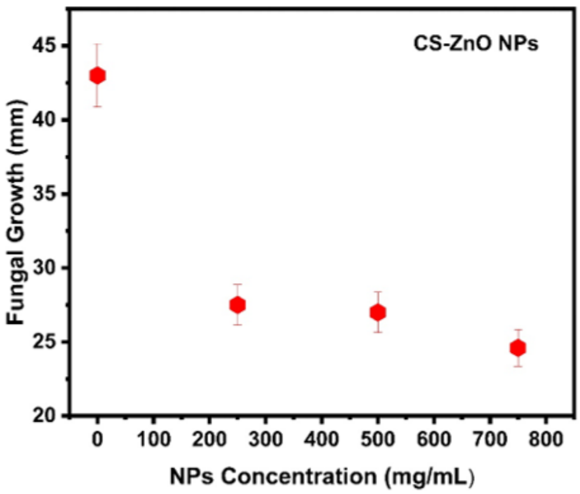

Figure 5. Antifungal activity CS-ZnO NPs against Alternaria solani

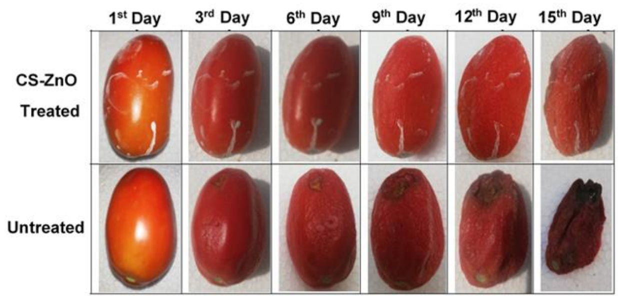

Figure 6. Preservation of tomatoes utilizing CS-ZnO NPs

3.5. Antifungal activity

Metals-based NPs, including silica, selenium, silver, and copper have been extensively used for the biological control of *Alternaria solani*, which caused early blight diseases (Ismail *et al*. 2016; Lahuf *et al*. 2020; Quiterio-Gutiérrez *et al*. 2019; Singh *et al*. 2022). This study employed CS-ZnO NPs biocontrol against the same fungus. The antifungal efficacy of CS-ZnO NPs was examined using agar well diffusion, revealing significant impact. As the concentration of CS-ZnO NPs increases the growth of *Alternaria solani* decreases. At 0 mg/mL, 250 mg/mL, 500 mg/mL, and 750 mg/mL concentrations of CS-ZnO NPs, the observed growth rate was calculated to be 43 mm, 27.5 mm, 27 mm, and 24.6 mm respectively as shown in figure 5. These concentrations notably affected the growth of *Alternaria solani*. Increasing NPs doses, as suggested by prior research, put impact on the growth and dissemination of fungal pathogen (Munnawar *et al*. 2017; Sukhodub *et al*. 2022).

3.6. Food preservation

For food preservation, CS-ZnO NPs were applied on the surface of tomatoes. The primary external factor influencing tomatoes' acceptance in the market is their color, which changes as they ripen, more precisely, the amount of chlorophyll is reduced and the amount of lycopene is increased (Munaro *et al*. 2024; Pinheiro *et al*. 2013). Color can be expressed as L* indicating perceptual lightness. The tomato fruit parameter a* depicts the transformation from green (-a*) to red (+a*); rising a* values indicate a redder tomato surface and hence indicative of ripeness (Belović *et al*. 2015; Goyal *et al*. 2024). It was found that relative to an untreated tomato, whose L* values had been lower ranging from 23–31, the NPs-treated tomato exhibited a high 32-41 brightness (L*) that ranged from 32-41 and had nearly stayed constant during storage. It was determined that the (a*) value for the untreated tomatoes remained low, ranging between 34 and 43, while those treated with NPs displayed some fluctuation, between 32 and 45. The composition of CS-ZnO NPs performed better in terms of delaying ripening-related color changes. Firmness, another important feature, represents a measurement of fruit texture and is essential for consumer acceptance; customers admire firm items more highly than those with softer textures. Changes in turgor pressure, cell wall structure, and content are used to identify the softening (Saei *et al*. 2011; Yang *et al*. 2024). The NPs-treated tomato demonstrated hardness throughout the storage period. Hence, The CS-ZnO NPs are good candidates for tomato preservation. Both pH and titratable acidity are essential quality features. Tomato's pH is influenced by citric acid concentration, which adds to fruit flavor, pH increases and acidity decreases during ripening is connected to citric acid loss (Anthon & Barrett 2012; Pavarin *et al*. 2024). The NPs-treated tomato demonstrated pH value that ranged from 4.0 to 4.5, and acidity, with a citric acid, value of 0.6%. Lycopene concentration varies significantly with the crop ripening stage and growth circumstances (García-Betanzos *et al*. 2016; Hanjabam *et al*. 2024). The growing value of lycopene concentration with storage time was lower in NPs-treated tomatoes than in the non-treated ones. The tomato treated with NPs retained the color of the fruit for a longer period of time while the untreated tomato showed a greater rise in lycopene. Hence indicating that red color intensification occurred both outside and within the tomato fruit. The use of NPs had a beneficial influence on quality parameters associated with the practical preservation and prolonged the shelf life of tomatoes preserved in refrigeration at 12°C to 16°C due to a modification of the membrane characteristics, enabling a decrease in metabolic changes. Figure 6 shows the pictures of NPs-treated and untreated tomato over the period of 15 days. It can be seen the NPs-treated one stayed in better condition in comparison to the non-treated one.

4. Conclusions

CS-ZnO NPs were synthesized by utilizing the sol-gel technique. Structural and optical characterization confirmed the successful synthesis of NPs with an average crystallite size of 15 nm while SEM indicated the agglomerated NPs. Absorption features further confirmed the successful synthesis of CS-ZnO NPs. TGA indicated two step weight loss process and for the prepared and investigated composition of CS-ZnO NPs, this weight loss is significantly low. These characterizations confirmed that the prepared CS-ZnO NPs holds good optical and thermal properties to be utilized in real world applications. On application side, the prepared CS-ZnO NPs showed promising antibacterial activity while modest antifungal activity was also demonstrated. Both antibacterial and antifungal activities are susceptible to amplification through elevated NPs concentrations. Furthermore, these NPs holds promise in augmenting preservation quality and notably extending the shelf life of the tomatoes as observed in the current study.

Funding

Researchers supporting project number (RSP2024R470), King Saud University, Riyadh, Saudi Arabia.

Acknowledgments

The authors extend their appreciation to the Researchers supporting project number (RSP2024R470), King Saud University, Riyadh, Saudi Arabia.

Declaration of competing interest

The authors declare that they have no competing financial interests or personal relationships that could have appeared to influence the work reported in this paper.

References

Ahmad A.A. and Sarbon N.M. (2021). A comparative study: Physical, mechanical and antibacterial properties of bio-composite gelatin films as influenced by chitosan and zinc oxide nanoparticles incorporation. *Food Bioscience*, **43**, 101250.

Alhujaily M., Albukhaty S., Yusuf M., Mohammed M.K.A., Sulaiman G.M., Al-Karagoly H. and AlMalki F.A. (2022). Recent advances in plant-mediated zinc oxide nanoparticles with their significant biomedical properties. *Bioengineering*, **9**(10), 541.

Alshammari F.H. (2022). Physical characterization and dielectric properties of chitosan incorporated by zinc oxide and graphene oxide nanoparticles prepared via laser ablation route. Journal of Materials *Research and Technology*, **20**, 740–747.

Anthon G.E. and Barrett D.M. (2012). Pectin methylesterase activity and other factors affecting pH and titratable acidity in processing tomatoes. *Food Chemistry*, **132**(2), 915–920.

Arab-Bafrani Z., Zabihi E., Jafari S.M., Khoshbin-Khoshnazar A., Mousavi E., Khalili M. and Babaei A. (2021). Enhanced radiotherapy efficacy of breast cancer multi cellular tumor spheroids through in-situ fabricated chitosan-zinc oxide bio-nanocomposites as radio-sensitizing agents. *International Journal of Pharmaceutics*, **605**, 120828.

Belović M., Kevrešan Ž., Pestorić M. and Mastilović J. (2015). The influence of hot air treatment and UV irradiation on the quality of two tomato varieties after storage. *Food Packaging and Shelf Life*, **5**, 63–67.

Bilal Shahid M., Nadeem M., Anjum Murtaza M. and Nadeem Riaz M. (2022). Impact of thermo-sonication on antioxidant potential in juices of selected citrus varieties. *Asian Journal of Agriculture and Biology* (*Online*).

Bondarenko O., Juganson K., Ivask A., Kasemets K., Mortimer M. and Kahru A. (2013). Toxicity of Ag, CuO and ZnO nanoparticles to selected environmentally relevant test organisms and mammalian cells in vitro: a critical review. *Archives of toxicology*, **87**, 1181–1200.

Corazzari I., Nisticò R., Turci F., Faga M.G., Franzoso F., Tabasso S. and Magnacca G. (2015). Advanced physico-chemical characterization of chitosan by means of TGA coupled on-line with FTIR and GCMS: Thermal degradation and water adsorption capacity. *Polymer Degradation and Stability*, **112**, 1–9.

Dananjaya S.H.S., Kumar R.S., Yang M., Nikapitiya C., Lee J. and De Zoysa M. (2018). Synthesis, characterization of ZnO-chitosan nanocomposites and evaluation of its antifungal activity against pathogenic Candida albicans. *International journal of biological macromolecules*, **108**, 1281–1288.

Domyati D. (2024). Dielectric and optoelectronics properties of thin films based on chitosan containing titanium oxide/hematite and their potential for optoelectronics devices. *Journal of Materials Science: Materials in Electronics*, **35**(6), 406.

Dong W., Su J., Chen Y., Xu D., Cheng L., Mao L. and Yuan F. (2022). Characterization and antioxidant properties of chitosan film incorporated with modified silica nanoparticles as an active food packaging. *Food Chemistry*, **373**, 131414.

Farrukh Saleem M., Bilal Hafeez M., Ramzan Y. and Nadeem M. (2022). Impact of soil applied humic acid, zinc and boron supplementation on the growth, yield and zinc translocation in wheat. *Asian Journal of Agriculture and Biology* (*Online*).

Fayaz A.M., Balaji K., Girilal M., Yadav R., Kalaichelvan P.T. and Venketesan R. (2010). Biogenic synthesis of silver nanoparticles and their synergistic effect with antibiotics: a study against gram-positive and gram-negative bacteria. *Nanomedicine: Nanotechnology, Biology and Medicine*, **6**(1), 103–109.

Gao Y. and Wu Y. (2022). Recent advances of chitosan-based nanoparticles for biomedical and biotechnological applications. *International journal of biological macromolecules*, **203**, 379–388.

Garavand F., Cacciotti I., Vahedikia N., Rehman A., Tarhan Ö., Akbari-Alavijeh S. and Jafarzadeh S. (2022). A comprehensive review on the nanocomposites loaded with chitosan nanoparticles for food packaging. *Critical reviews in food science and nutrition*, **62**(5), 1383–1416.

Garavand F., Rouhi M., Razavi S.H., Cacciotti I. and Mohammadi R. (2017). Improving the integrity of natural biopolymer films used in food packaging by crosslinking approach: A review. *International journal of biological macromolecules*, **104**, 687–707.

García-Betanzos C.I., Hernández-Sánchez H., Quintanar-Guerrero D., Del Real L A. and de la Luz Zambrano-Zaragoza M. (2016). The evaluation of mechanical, thermal, optical and microstructural properties of edible films with solid lipid nanoparticles-xanthan gum stored at different temperatures and relative humidities. *Food and Bioprocess Technology*, **9**, 1756–1768.

Gasti T., Dixit S., Hiremani V.D., Chougale R.B., Masti S.P., Vootla, S.K. and Mudigoudra B.S. (2022). Chitosan/ pullulan based films incorporated with clove essential oil loaded chitosan-ZnO hybrid nanoparticles for active food packaging. *Carbohydrate Polymers*, **277**, 118866.

González-Campos J.B., Prokhorov E., Luna-Bárcenas G., Sanchez I.C., Lara-Romero J., Mendoza-Duarte M.E. and Guevara-Olvera L. (2010). Chitosan/silver nanoparticles composite: Molecular relaxations investigation by dynamic mechanical analysis and impedance spectroscopy. *Journal of Polymer Science Part B: Polymer Physics*, **48**(7), 739–748.

Goyal K., Kumar P. and Verma K. (2024). Tomato ripeness and shelf-life prediction system using machine learning. *Journal of Food Measurement and Characterization*, 1–16.

Hanjabam J.S., Devi M.A., Singh S.G., Brahmacharimayum N. and Devi O.S. (2024). Extensive research on how extraction method, heat treatment and the storage condition affect the lycopene content of various foods. *Journal of Population Therapeutics and Clinical Pharmacology*, **31**(1), 1467–1493.

Iqbal T., Raza A., Zafar M., Afsheen S., Kebaili I. and Alrobei H. (2022). Plant-mediated green synthesis of zinc oxide nanoparticles for novel application to enhance the shelf life of tomatoes. *Applied Nanoscience*, 1–13.

Islam M.F., Miah M.A.S., Huq A.K.O., Saha A.K., Mou Z.J., Mondol M.M.H. and Bhuiyan M.N.I. (2024). Green synthesis of zinc oxide nano particles using Allium cepa L. waste peel extracts and its antioxidant and antibacterial activities. *Heliyon*, **10**(3).

Ismail A.-W., Sidkey N., Arafa R., Fathy R. and El-Batal A. (2016). Evaluation of in vitro antifungal activity of silver and selenium nanoparticles against Alternaria solani caused early blight disease on potato. *British Biotechnology Journal*, **12**(3), 1–11.

Khazaal F.A., Kadhim M.M., Husseein H.F., Abbas Z.M., Shamzah M., Khudhair I.A. and Saieed H.S. (2020). Electronic transfers and (nlo) properties predicted by ab initio methods with prove experimentally. *NeuroQuantology*, **18**(1), 46.

Lahuf A.A., Abdullah K.M. and Mohammadali M.T. (2020). Assessment of the nanosized particles of ZnO and MgO and some cultivars in control of Alternaria solani causing tomato early blight. *Ecology, Environment and Conservation*, **26**, 89–95.

Li Y., Zhou Y., Wang Z., Cai R., Yue T. and Cui L. (2021). Preparation and characterization of chitosan–nano-ZnO composite films for preservation of cherry tomatoes. *Foods*, **10**(12), 3135.

Madhan G., Begam A.A., Varsha L.V., Ranjithkumar R. and Bharathi D. (2021). Facile synthesis and characterization of chitosan/zinc oxide nanocomposite for enhanced antibacterial and photocatalytic activity. *International journal of biological macromolecules*, **190**, 259–269.

Magesh G., Bhoopathi G., Nithya N., Arun A.P. and Kumar E.R. (2018). Tuning effect of polysaccharide chitosan on structural, morphological, optical and photoluminescence properties of ZnO nanoparticles. *Superlattices and Microstructures*, **117**, 36–45.

Malik I.R., Nayyab S., Mirza M.R., Muzammil S., Cheema J.S., Imran K. and Javed M. (2022). Growth performance of major carps during exposure of zinc and bioaccumulation in fish body organs.

Medina E., Caro N., Abugoch L., Gamboa A., Díaz-Dosque M. and Tapia C. (2019). Chitosan thymol nanoparticles improve the antimicrobial effect and the water vapour barrier of chitosan-quinoa protein films. *Journal of Food Engineering*, **240**, 191–198.

Mirzaei-Mohkam A., Garavand F., Dehnad D., Keramat J. and Nasirpour A. (2019). Optimisation, antioxidant attributes, stability and release behaviour of carboxymethyl cellulose films incorporated with nanoencapsulated vitamin E. *Progress in Organic Coatings*, **134**, 333–341.

Muhammad S., Muhammad A. and Usman Ghani M. (2022). Phenotypic evaluation of rice germplasm against Xanthomonas oryzae pv. oryzae and its in-vitro management through antibiotics. *Asian Journal of Agriculture and Biology* (Online).

Muiz L.J., Juwono A.L. and Krisnandi Y.K. (2022). A review: Silver–zinc oxide nanoparticles–organoclay-reinforced chitosan bionanocomposites for food packaging. *Open Chemistry*, **20**(1), 1155–1170.

Munaro D., Mazo C.H., Bauer C.M., da Silva Gomes L., Teodoro E. B., Mazzarino L. and Maraschin M. (2024). A novel biostimulant from chitosan nanoparticles and microalgae-based protein hydrolysate: Improving crop performance in tomato. *Scientia Horticulturae*, **323**, 112491.

Munnawar I., Iqbal S.S., Anwar M.N., Batool M., Tariq S., Faitma N. and Jamil T. (2017). Synergistic effect of Chitosan-Zinc Oxide Hybrid Nanoparticles on antibiofouling and water disinfection of mixed matrix polyethersulfone nanocomposite membranes. Carbohydrate Polymers, **175**, 661–670.

Nandana C.N., Christeena M. and Bharathi D. (2021). Synthesis and characterization of chitosan/silver nanocomposite using rutin for antibacterial, antioxidant and photocatalytic applications. *Journal of Cluster Science*, 1–11.

Nandiyanto A.B.D., Oktiani R. and Ragadhita R. (2019). How to read and interpret FTIR spectroscope of organic material. *Indonesian Journal of Science and Technology*, **4**(1), 97–118.

Pavarin F.F.A., Fracarolli J.A. and Falcão A.X. (2024). Biospeckle laser for assessing tomatoes ripeness indexes. *Revista Ciência Agronômica*, **55**, e20207677.

Pholnak P., Khongbun J., Suksom K., Lertworapreecha M., Suwanboon S. and Sirisathitkul C. (2020). Antifungal efficacy of chitosan-modified zinc oxide nanoparticles on tube sedge products. *Journal of Nanostructures*, **10**(2), 424–433.

Pinheiro J., Alegria C., Abreu M., Gonçalves E.M. and Silva C.L.M. (2013). Kinetics of changes in the physical quality parameters of fresh tomato fruits (Solanum lycopersicum, cv. Zinac') during storage. *Journal of Food Engineering*, **114**(3), 338–345.

Prokhorov E., Luna-Bárcenas G., Yáñez Limón J.M., Gómez Sánchez A. and Kovalenko Y. (2020). Chitosan-ZnO nanocomposites assessed by dielectric, mechanical, and piezoelectric properties. *Polymers*, **12**(9), 1991.

Quiterio-Gutiérrez T., Ortega-Ortiz H., Cadenas-Pliego G., Hernández-Fuentes A.D., Sandoval-Rangel A., Benavides-Mendoza A. and Juárez-Maldonado A. (2019). The application of selenium and copper nanoparticles modifies the biochemical responses of tomato plants under stress by Alternaria solani. *International journal of molecular sciences*, **20**(8), 1950.

Ramezani M., Ramezani F. and Gerami M. (2019). Nanoparticles in pest incidences and plant disease control. *Nanotechnology for agriculture: crop production & protection*, 233–272.

Rilda Y., Ayuni P.V.P., Refinel R., Armaini A., Agustien A., Almurdi A. and Pardi H. (2022). Antibacterial properties and uv-protection of cotton fabric using nanohybrid multilayer zno-sio$_2$/chitosan and dodecyltrietoxysilane (DTS). *Rasayan Journal of Chemistry*, **15**(1).

Rumi M.J.U. and Rahman M.M. (2023). Influence of alumina and zinc oxide nanoparticles on microstructure and electro-mechanical properties of aluminum metal matrix composites fabricated by customized two-step stir casting method.

Saei A., Tustin D.S., Zamani Z., Talaie A. and Hall A.J. (2011). Cropping effects on the loss of apple fruit firmness during storage: The relationship between texture retention and fruit dry matter concentration. *Scientia Horticulturae*, **130**(1), 256–265.

Shaukat N., Farooq U., Akram K., Shafi A., Hayat Z., Naz A. and Khan M.Z. (2023). Antimicrobial potential of banana peel: a natural preservative to improve food safety.

Singh A., Gaurav S.S., Shukla G. and Rani P. (2022). Assessment of mycogenic zinc nano-fungicides against pathogenic early blight (Alternaria solani) of potato (Solanum tuberosum L.). *Materials Today: Proceedings*, **49**, 3528–3537.

Singh A., Singh N. á., Afzal S., Singh T. and Hussain I. (2018). Zinc oxide nanoparticles: a review of their biological synthesis, antimicrobial activity, uptake, translocation and biotransformation in plants. *Journal of materials science*, **53**(1), 185–201.

Sukhodub L., Kumeda M. and Sukhodub L. (2022). Effect of Metal Ions on the Porosity and Antimicrobial Properties of ZnO-Alginate-Chitosan Composites. *International Conference on Nanotechnology and Nanomaterials*

Tamanna N.J., Hossain M.S., Bahadur N.M. and Ahmed S. (2024). Green synthesis of Ag_2O & facile synthesis of ZnO and characterization using FTIR, bandgap energy & XRD (Scherrer equation, Williamson-Hall, size-train plot, Monshi-Scherrer model). *Results in Chemistry*, **7**, 101313.

Thirumavalavan M., Huang K.-L. and Lee J.-F. (2013). Preparation and morphology studies of nano zinc oxide obtained using native and modified chitosans. *Materials*, **6**(9), 4198–4212.

Verma Y., Singh S.K., Jatav H.S., Rajput V.D. and Minkina T. (2022). Interaction of zinc oxide nanoparticles with soil: Insights into the chemical and biological properties. *Environmental Geochemistry and Health*, 1–14.

Wang Y., Dong S., Li X., Hong C. and Zhang X. (2022). Synthesis, properties, and multifarious applications of SiC nanoparticles: A review. *Ceramics International*, **48**(7), 8882–8913.

Wasilewska A., Klekotka U., Zambrzycka M., Zambrowski G., Święcicka I. and Kalska-Szostko B. (2023). Physico-chemical properties and antimicrobial activity of silver nanoparticles fabricated by green synthesis. *Food Chemistry*, **400**, 133960.

Yang F., Zhao R., Suo J., Ding Y., Tan J., Zhu Q. and Ma Y. (2024). Understanding quality differences between kiwifruit varieties during softening. *Food Chemistry*, **430**, 136983.

Yempally S., Cabibihan J.J. and Ponnamma D. (2024). A Facile Approach to Develop Polyvinyl Alcohol-Based Bio-Triboelectric Nanogenerator Containing Graphene-Doped Zinc Oxide Quantum Dots. *Energy Technology*, 2300992.

Yue L., Wang M., Khan I.M., Niazi S., Wang B., Ma X. and Xia W. (2021). Preparation and characterization of chitosan oligosaccharide derivatives containing cinnamyl moieties with enhanced antibacterial activities. LWT, **147**, 111663.

Zaman H.G., Baloo L., Aziz F., Kutty S.R. and Ashraf A. (2022). COD adsorption and optimization from produced water using chitosan–ZnO nanocomposite. *Applied Nanoscience*, **12**(6), 1885–1898.